EPJ Web of Conferences **29**, 00004 (2012)
DOI: 10.1051/epjconf/20122900004

Effect of Fe doping on properties of $Pr_{0.67}Ba_{0.33}Mn_{1-x}Fe_xO_3$ perovskites

M. Baazaoui[a1,2], M. Boudard [2], S. Zemni 1[a], V. Nassif [3,4], F. Gay [3], M. Oumezzine [1]

[1]Laboratoire de Physico–Chimie des Matériaux, Faculté des Sciences de Monastir, Département de Physique, 5019, Université de Monastir, Monastir, Tunisie.
[2]Laboratoire des Matériaux et du Génie Physique (CNRS UMR 5628), Minatec Bâtiment INPG, parvis Louis Néel, BP 257, 38016 Grenoble Cedex 1, France.
[3]Institut Néel (CNRS and UJF), BP 166, 38042 Grenoble Cedex 9, France
[4]Institut Laue Langevin, BP 156, 38042 Grenoble Cedex 9, France

Abstract. Changes in the physical properties of ceramic $Pr_{0.67}Ba_{0.33}Mn_{1-x}Fe_xO_3$ ($0 \leq x \leq 0.15$) are interpreted as resulting from the suppression of the ferromagnetic double exchange interaction with almost no lattice effect due to similar ionic radii value of Fe^{3+} and Mn^{3+} Magnetization and transport measurements show at low temperature ferromagnetic and metallic behavior for x=0 and 0.05 samples, whereas x = 0.10 and x = 0.15 compounds show spin glass like and semiconducting behavior. At high temperature semiconductor and paramagnetic behavior are observed for all the samples.
Keywords: Magnetic materials; X-ray diffraction; Physical properties.
PACS: 61, 75

1 Introduction

Manganites perovskite oxides were widely studied in the last two decades after the discovery of colossal magnetoresistance (CMR) [1]. Below the Curie temperature (T_C) ferromagnetic (FM) and metallic behavior (obtained by creation of mixed Mn^{3+}/Mn^{4+} valence when doping) were explained within the double exchange (DE) mechanism [2]. Polaronic type model [3] or segregation phase models [4, 5] were then introduced to fully explain the transport behavior above T_C and the CMR properties.

Among divalent doped systems, those with Ba content remains less investigated despite the initial discovery of the CMR effect in $La_{0.67}Ba_{0.33}MnO_3$ thin films [6] (see [4] and [7] and references therein). Recently we have investigated $La_{0.67}Ba_{0.33}Mn_{1-x}TM_xO_3$ systems with TM=Ti^{4+} [7] and Fe^{3+} [8]. The effect of trivalent magnetic (Fe^{3+}) or tetravalent non- magnetic (Ti^{4+}) substitution for Mn on magnetic and electrical properties [7- 9] appears quite similar in both systems and eliminates the ferromagnetic/metallic (FM/M) and paramagnetic/ insulator (PM/I) transitions in these systems. More recently we have shown that the $Pr_{0.67}Ba_{0.33}Mn_{1-x}Fe_xO_3$ iron doped systems presents very interesting magnetocaloric properties [10]. In this paper we report in more details its structural, magnetic and electrical properties that appear quite similar to previous Ba-doped studied system.

[a] e-mail : medbaazaoui@yahoo.fr

2 Experimental

Samples with nominal compositions $Pr_{0.67}Ba_{0.33}Mn_{1-x}Fe_xO_3$ ($0 \leq x \leq 0.15$) were prepared by solid state reaction using Pr_6O_{11}, $BaCO_3$, Mn_2O_3 and Fe_2O_3 with similar thermal treatment as the one used in [8, 9]. The samples are finally annealed at 1453 K for 24h in air. Microstructure and composition of the samples were studied by scanning electron microscopy (SEM) using a Philips XL30 microscope with an energy dispersive X-ray (EDX) spectrometer working at 20 kV. Powder X-ray diffraction (XRD) were collected using Co-Kα radiation in the 2θ range 20° - 100° with a step size of 0.017° and a counting time of 18 s per step at room temperature (RT). Powder neutron diffraction (PND) experiment was carried out at Institut Laue Langevin on D1B diffractometer using 2.52Å wavelength and a multidetector covering a 2θ angular range from 37°– 117° at RT. Rietveld structure refinement was carried out using the FULLPROF software [11]. Magnetization *(M)* was measured using a linear extracting magnetometer. Temperature dependence *(M (T))* was measured either with zero field cooled (ZFC)) and field cooled (FC) samples. Applied magnetic field (*M (H)*) dependence was measured at 10K up to *H*=100 kOe. Transport properties were measured by four probe methods.

3 Results and discussion

3.1. Microstructure and structural analyses

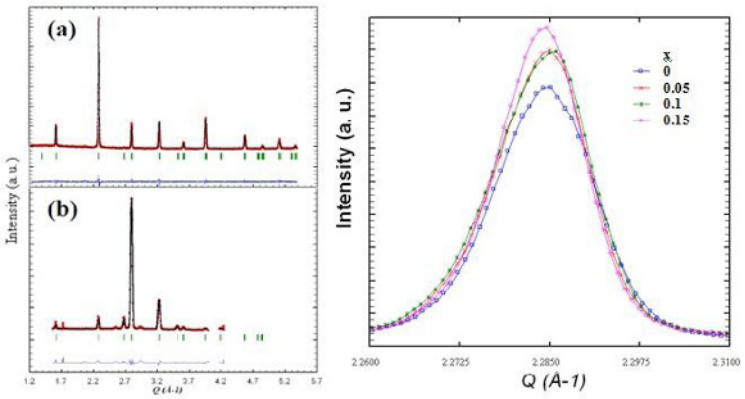

Fig 1. (a) XRD and ((b) PND Rietveld refinement results for sample with x = 0.05 at RT. The difference between measured (red) and calculated data (black) is plotted below (blue). Vertical green lines correspond to Bragg positions. (c) XRD shows a negligible shift of the most intense peak when Fe amount increases.

SEM, XRD and PND observations show for all the samples a unique phase with 1 to 2 μm average grain size. EDX observations on 100μm×100μm regions show that Pr, Ba, Mn and Fe compositions are close to the nominal ones. Only slight structural modifications are observed by XRD and PND on Fe doping (see peak position evolution on Fig. 1 (c)). Indexing of the diffractograms and Rietveld structure refinements was performed using orthorhombic Imma symmetry [12, 13].

The (Pr, Ba) atoms are at 4e (0, 1/4, z) position, (Mn, Fe) at 4b (0, 0, 1/2), O (1) at 4e (0, ¼, z) and O (2) at 8g (1/4, -y, 3/4). Refinement results are listed in table 1, and show that the average structure as a function of Fe substitution appears almost constant as expected from similar ionic radii of Fe^{3+} and Mn^{3+} ions (0.645Å [14]).

Table 1. Structural parameters for XRD and PND Rietveld refinement for $Pr_{0.67}Ba_{0.33}Mn_{1-x}Fe_xO_3$ at RT (Imma space group). V is the cell volume; B_{iso} is the overall isotropic thermal parameter; TM-O the bond lengths between TM=(Mn,Fe) and O and TM-O-TM are the bond angles, G_s is the average grain size. R_{wp}, R_p and R_F are the agreement factors for the weighted profiles, the profiles and the structure factors; χ^2 is the goodness of fit. The numbers in parentheses are estimated standard deviations to the last significant digit.

	x					
	0	**0**	**0.05**	**0.1**	**0.15**	**0.15**
Diffraction	XRD	PND	XRD	XRD	XRD	PND
Cell parameters						
a(nm)	0.550037(2)	0.55028(4)	0.550062(3)	0.549935(3)	0.550084(3)	0.55213(3)
b(nm)	0.776402(4)	0.78089(4)	0.776633(4)	0.776676(4)	0.776855(3)	0.77809(4)
c(nm)	0.551929(4)	0.55084(4)	0.552185(2)	0.552247(2)	0.552184(2)	0.55108(3)
V(nm^3)	0.23570(2)	0.2367(2)	0.23589(1)	0.23588(1)	0.23597(1)	0.2368(1)
Atoms						
Pr/Ba z	0.003(1)	0.034(2)	0.004(1)	0.0010(1)	0.003(1)	0.035(2)
$B_{iso}(nm^2)$	0.0046(3)	0.001947	0.0063(3)	0.0059(3)	0.0066(3)	0.006(4)
Mn/Fe $B_{iso}(nm^2)$	0.0011(3)	0.0028833	0.0060(5)	0.0042(5)	0.0078(4)	0.0024403
O(1) z	0.56	0.56	0.56	0.56	0.562(2)	0.56
$B_{iso}(nm^2)$	0.01	0.01	0.01	0.01	0.01	0.01
O(2) y	-0.00061	-0.0006	-0.0006	-0.00073	-0.00088	-0.00088
$B_{iso}(nm^2)$	0.02	0.02	0.02	0.02	0.02	0.02
Structural parameters						
TM-O(1) (nm)	0.1969052	0.198	0.1969647	0.1969759	0.19721	0.197313
TM-O(2) (nm)	0.1948028	0.194653	0.1948527	0.1948413	0.1948568	0.195023
TM-O(1)-TM (°)	160.6358	160.782	160.6327	160.6316	160.01	160.706
TM-O(2)-TM (°)	179.7223	179.725	179.6816	179.6672	179.5970	179.635
G_s(nm)	48.5	-	54.86	52.46	60.61	-
Agreement factors						
R_{wp}(%)	2.00	4.15	1.98	2	1.80	3.74
R_p(%)	1.48	2.79	1.44	1.47	1.37	2.51
R_F(%)	4.90	2.12	3.97	4.60	3.13	2.01
χ^2	1.51		1.53	1.55	1.23	

The average crystallites sizes obtained from the XRD refinement are reported in table 1 and range from 48 - 61 nm. These values are much lower than the micrometer size of grains observed by SEM indicating an intrinsic disorder within the grains. This point could affect to some extent the magnetic and electrical properties.

3.2 Magnetic Properties

M(T) curves measured at constant magnetic field of 500 Oe and *M(H)* measurements at 10K are shown in Fig. 2.

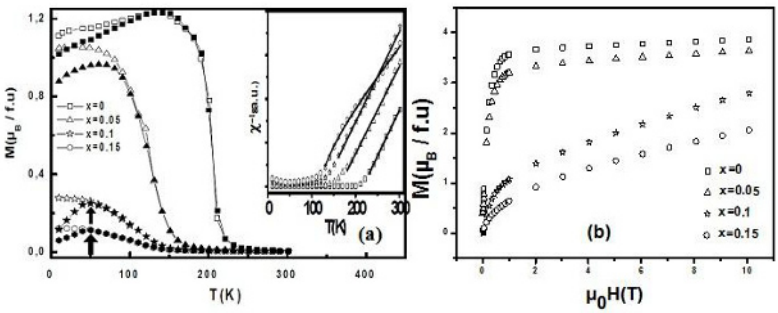

Fig. 2. Magnetic measurements for $Pr_{0.67}Ba_{0.33}Mn_{1-x}Fe_xO_3$. (a) *M (T)* curves at μ_0H = 500 Oe magnetic field in FC (open symbols) and ZFC (close symbols). The arrows indicate *Tm* for x = 0.1 and 0.15 Fe amount. The inset shows the inverse of magnetic susceptibility ($1/\chi$) vs. T plots and the black solid line in these plots represents the fit of the high-T region (see text). (b) *M (H)* curves at 10K.

These results show for x = 0 and x = 0.05 samples a clear PM to FM phase transition resulting in an increase of *M* at low T in Fig.2 (a). The corresponding *M(H)* curves at 10K (Fig. 2 (b)) show a typical FM regime with a sharp increase of *M* at low field corresponding to rearrangement of ferromagnetic domains. *M* reaches rapidly an almost constant value for higher fields corresponding to parallel alignment of the spins. In the following *M* measured in 100 kOe at 10 K will be identified with the saturation magnetization M_s^{meas}. The measured saturation moment expressed in Bohr magneton per atomic formula unit $\mu_s^{meas} = M_s^{meas} M_m / N_a \mu_B$ (with N_a the Avogadro number, M_m the molecular mass per unit formula and μ_B the Bohr magneton) is given in table 2. For samples with x μ0.05, μ_s^{meas} can be compared with the moment μ_s^{cal} calculated for a full spin alignment in the limit T = 0K. The μ_s^{cal} values given in table 2 have been obtained assuming only Mn and Fe ferromagnetic contribution with a quenched orbital moment, S =2 for Mn^{3+}, S =3/2 for Mn^{4+}, S = 5/2 for Fe^{3+} and g = 2 for both Mn^{3+}, Mn^{4+} and Fe^{3+}. The Mn^{3+} and Mn^{4+} concentrations (also given in table 2) are deduced from the composition of the manganite phase under the assumption of substitution of Mn^{3+} by Fe^{3+}. The observed and calculated moments coincide reasonably, which confirms that, despite Fe substitution, a FM state is present in samples with $x \leq 0.05$. Note that this comparison can only be taken as qualitative since a more complicated magnetic state should be probably taken into account. Furthermore the unavoidable uncertainties on the O content lead to large variations in the Mn^{3+} and Mn^{4+} concentrations and strongly affect the calculated moment. Finally we noted that the ferromagnetic regime observed for x = 0 sample shows a slightly unsaturated magnetization corresponding to realignment of the spins induced by the external field that could be due either to canted long range ordering of the Mn/Pr spins and/or to a magnetic disorder state of Pr (in this scenario the external field induces an additional polarization of Pr superimposed to the one due to the internal field due to Mn spins).

A reasonable estimation of the Curie temperature T_C can be obtained by determining the temperature of the maximum of d*M(T)*/d*T* (table 2). Our T_C value for undoped compound, 205K, is close to that reported in the literature ranging from 167K to 195 K (T_C = 180 K [13] and T_C = 167 K [15]) and a decrease of T_C is observed for x=0.05 doped sample. Substitution of Fe at the Mn site weakens the FM interactions and reduces both T_C and μ_s^{meas} (see table 2).

Table 2. Magnetic transition temperature T_C or T_m (see text) for $Pr_{0.67}Ba_{0.33}Mn_{1-x}Fe_xO_3$ samples. Experimental and calculated magnetic saturation moments μ_S^{meas} and μ_S^{cal}. Curie Weiss temperature Θ, experimental (μ_{eff}^{meas}) and calculated (μ_{eff}^{th}) effective paramagnetic moments.

x	T_C or T_m (K)	μ_S^{cal}(μ_B/f.u.)	μ_S^{meas}(μ_B/f.u.)	Θ(K)	μ_{eff}^{meas}(μ_B)	μ_{eff}^{th}(μ_B)
0	205	3.67	3.86	215	7.25	5.44
0.05	128	3.72	3.63	155	7.77	5.49
0.1	50	3.77	2.79	134	5.69	5.44
0.15	50	3.82	2.05	112, -16	7.10	5.59

For x = 0.1 and 0.15 samples the *M(T)* curves in Fig.2 (a) have no sharp increase and a low *M* magnitude. The temperature (T_m = *50 K*) reported in table 2 corresponds to the maximum value of the ZFC curve. At T_m, a bifurcation between the FC and ZFC curves (λ shape) is observed which is generally associated in the literature of manganites with a magnetic glass state (cluster or spin - glass [16]). *M(H)* measurements at 10 K (see Fig. 2 (b)) show that *M* for x = 0.1 and 0.15 do not exhibit a FM regime as there is neither a sharp increase and nor a saturation value of *M* with the applied field that could correspond to parallel spin alignment.

The inverse of the susceptibility (calculated from data of Fig. 2 (a)) is shown in the inset, as a function of temperature in the PM region (above T_C or T_m). It can be generally fitted by a Curie Weiss law: $\chi=\frac{C}{T-\Theta}$ with Θ the Curie Weiss temperature and C the Curie constant defined as $C=\frac{1}{3k_B}\frac{N_a}{M_m}\mu_{eff}^{meas^2}\mu_B{}^2$, k_B the Boltzmann constant, and μ_{eff}^{meas} the effective moment expressed in Bohr magnetons. The obtained Θ values (see table 2) are generally positive and decrease with Fe content following the same trend as T_C or T_m. The positive value of Θ confirms a mean FM interaction between spins for all samples. One can compare the measured effective moment with the calculated one $\mu_{eff}{}^{th}=\sqrt{\sum_i c_i \mu_i{}^2}$, using cation concentrations (c_i) and individual cation theoretical effective paramagnetic moment (μ_i). One finds that for FM x=0 and x = 0.05 samples the measured effective magnetic moments in the PM regime are significantly larger than the calculated ones. This result is commonly observed in manganites (see by example Blanco et al. [17, 18] and is generally attributed to the existence of short range FM interactions above T_C. For the non FM x = 0.1 and x = 0.15 samples a different behaviour is observed. For sample with x = 0.1 (inset of Fig. 2 (a)) we observed a linear behaviour well above T_m with a value of μ_{eff}^{meas} almost equal to the theoretical value μ_{eff}^{th} appearing as a normal PM region whereas a complex behaviour is observed for sample with x=0.15 above T_m. This type of curve is commonly observed in manganites and is generally explained as arising from inhomogeneous systems (phase segregation) that are believed to be the key for understanding CMR properties [4, 5]. A deviation from the linear paramagnetic region [180 K-300 K] is observed below 180K and the data can be fitted in this region [130 K-300 K] by considering a two phases models (FM, AFM contributions) with two distinct transition temperatures, Θ_F and Θ_N following $\chi=\beta\frac{C}{T-\Theta_F}+(1-\beta)\frac{2C}{T-\Theta_N}$ where β (fixed to 0.5) corresponds to the proportion of the AFM phase with negative Néel transition temperature Θ_N. Results of this fit are indicated by solid lines in the inset of Fig. 2 and in Table 2 (Θ_N is indicated by the negative value). The negative value of Θ_N and the reduction (inset of Fig. 2 (a)) of the slope, corresponding to the coefficient 2C, are strong indications of AFM contribution in this sample and a phase separation [4, 5] tendency of the system beyond 10% of Fe amount is expected.

Further experiments are necessary to fully understand how Fe doping affects the magnetic state of these samples but strong indication of AFM and FM competing interaction is expected from our observations for x = 0.15 sample. Indeed local AFM superexchange interactions between Fe and Mn ions are expected in our system as no competing DE (FM) interactions are possible [19-21]. This point is confirmed by our M_s^{meas} value for x=0.05 lower than the one for x=0 whereas a larger value would be expected for a FM full spin alignment (Fe^{3+} contributes with 5μB whereas Mn^{3+} contributes with 4μB). Blanco et al. reported spin glass behavior arising from competing FM and AFM interactions in $Nd_{0.7}Pb_{0.3}Mn_{1-x}Fe_xO_3$ [17, 18] system. In particular sample with Fe content x = 0.075 in their Fig. 3 shows a behavior reminiscent of FM to AFM phase transition (typically observed in $Pr_{0.5}Sr_{0.5}MnO_3$ [22]) and their $Nd_{0.7}Pb_{0.3}Mn_{0.9}Fe_{0.1}O_3$ sample presents very similar λ shape as our non FM samples. A complex magnetic state due to a mixture of AFM and FM sate is observed for $Pr_{0.67}Ca_{0.33}MnO_3$ sample [23].

3.3 Transport properties

Fig. 3 shows the transport properties for selected samples (x = 0, x = 0.05 and x = 0.15). The samples with x = 0 and x = 0.05 exhibit a metallic behaviour at low temperature. For these samples a phase transition from metallic to a high temperature semiconducting state is characterized by a maximum resistance at temperature T_P indicated by arrows in Fig. 3. For x = 0 sample this value of T_P is lower than T_C (68 K temperature difference between T_C (205 K) and T_P (137 K) for x = 0) and for comparison no clear transition was observed in *M(T)* curve in ref. [13] where T_P = 120 K for x = 0). For our samples T_P decreases with the increase of Fe content (T_P = 137 K for x = 0 and T_P = 75 K for x = 0.05) which can be directly related to a decrease of the ratio of Mn^{3+}/Mn^{4+} that weakens the Mn^{3+}-O-Mn^{4+} DE FMM interactions [19, 24] (Fe^{3+}-O-Fe^{3+} and Mn^{3+}-O-Fe^{3+} do not allow active DE).

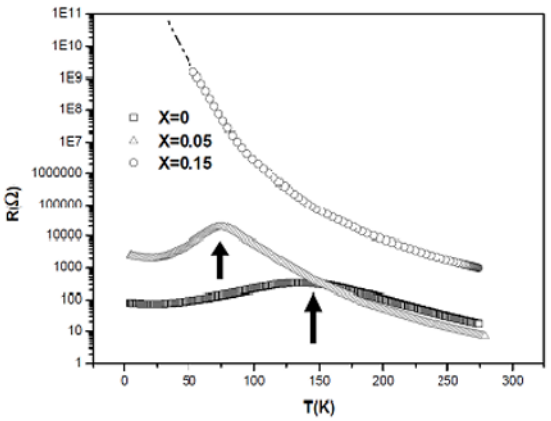

Fig. 3. Zero field resistance vs. temperature curves for $Pr_{0.67}Ba_{0.33}Mn_{1-x}Fe_xO_3$ (x = 0, x = 0.05 and x = 0.15) samples. The arrows indicate the metal-insulator phase transition

For the x = 0.15 sample the decrease of the ratio of Mn^{3+}/Mn^{4+} appears to be too important to retain a metallic state: a semiconducting behavior is observed in all the temperature range. Consequently, the doping of Fe in these manganites $Pr_{0.67}Ba_{0.33}Mn_{1-x}Fe_xO_3$ (x = 0- 0.15) results in a reduction in the number of available hopping electron, which removes the metallicity and establishes semiconducting behavior.

4. Conclusions

We have studied the effect of Fe doping at Mn- site on electrical and magnetic properties of $Pr_{0.67}Ba_{0.33}Mn_{1-x}Fe_xO_3$ ($0 \leq x \leq 0.15$) manganese oxide. Powder XRD and PND structure analysis and morphological investigation have shown that structural parameters and grain sizes are almost not affected by Fe doping. Magnetic and electrical measurements show a FMM - PMI transition with a reduction in both T_C and T_P and a decrease (respectively an increase) of the magnetization (respectively of the resistivity) with increasing Fe content. No FMM-PMI transition was observed above 10% Fe amount. In the PM region, the two FM samples (x = 0 and 0.05) present short range FM interactions above T_C. The x = 0.1 sample presents a normal PM behavior, whereas for x = 0.15 sample the data were well fitted by considering two Curie laws corresponding to FM and AFM behaviors with two distinct transition temperatures, Θ_F and Θ_N. ZFC *M(T)* measurements is compatible with a magnetic glass state below 50 K for x = 0.1 and 0.15 compounds. *M(H)* measurements at 10K show that the materials with 0 and 5% Fe^{3+} content, exhibit FM behavior while beyond that concentration there is probably a competition of both FM and AFM behaviours. Changes in these properties have been analyzed on the basis that the substitution of Fe^{3+} for Mn^{3+} reduces the double exchange (DE) FMM interaction.

Acknowledgments

Institut Laue Langevin is kindly acknowledged for help and allocation of beam time for neutron diffraction experiment. M. Baazaoui gratefully thanks the region Rhône-Alpes for allocation of a TEMPRA Grant.

References

1. R. Von Helmolt, J. Wecker, B. Holzapfel, L. Schultz, K. Samwer, Phys. Rev. Lett.**71** (1993) 2331-2333.
2. C. Zener, Phys. Rev. **82** (1951) 403–405. P.W. Anderson, H. Hasegawa, Phys. Rev. **100** (1955) 675–681.P.G. Degennes, Phys. Rev. **118** (1960) 141.
3. A.J. Millis, P.B. Littlewood, B.I. Chairman, Phys. Rev. Lett. **74**, (1995) 5144–5147.
4. E. Dagotto, T. Hotta, A. Moreo, Phys. Rep. **344** (2001) 1-153.
5. M. Tovar, M.T. Causa, C.A. Ramos, D. Laura-Ccahuana, J. Magn. Magn. Mater. **320** (2008) 523-527.
6. M. P. Brown and K. Austin, The New Physique, Publisher City: Publisher Name, 2005, pp. 25-30.
7. A. Gasmi, M. Boudard, S. Zemni, F. Hippert and M. Oumezzine, J. Phys. D: Appl. Phys. **42** (2009) 225408 (7pp).
8. M. Baazaoui, S. Zemni, M. Boudard, H. Rahmouni, A. Gasmi, A. Selmi, M. Oumezzine Mater. Lett. **63** (2009) 2167-2170.
9. M. Baazaoui, S. Zemni, M. Boudard, H. Rahmouni, M. Oumezzine A. Selmi, Physica B **405** (2010) 1470–1474.
10. M. Baazaoui, M. Boudard, S. Zemni, Mater. Lett. **65** (2011) 2093-2095.
11. R. A. Young, the Rietveld Method, Oxford University Press, New York, 1993. J. Rodriguez-Carvajal, FULLPROF, LLB Saclay, France, 2001.
12. F. Damay, Z. Jirak, M. Hervieu, C. Martin, A. Maignan, B. Raveau,G. André, F. Bourée, J. Magn. Magn. Mat. **190** (1998) 221-232.
13. A. K. Heilman, Y.Y. Xue, B. Lorenz, B.J. Campbell, J. Cmaidalka, R.L. Meng, Y.S. Wang, C.W. Chu, Phys. Rev. B **65** (2002) 214423-214425.
14. R. D. Shannon, Acta Crystallogr. A **32** (1976) 751-764.
15. D. C. Krishna, P. Venugopal Reddy, J. Alloy. Compd. **479** (2009) 661–669.
16. J. A. Mydosh, in Spin Glass: An experimental Introduction, Taylor & Francis ed., London, 1993.
17. J. J. Blanco, M. Insausti, I. Gil de Muro, L. Lezama, T. Rojo, J. Sol. Stat. Chem. **179** (2006) 623-631.
18. J.J. Blanco, L. Lezama, M. Insausti, J. Gutierrez, J.M. Barandiaran, T. Rojo, Chem. Mater. **11** (1999) 3464-3469.
19. A. G. Mostafa, E.K. Abdel-Khalek, W.M. Daoush, S.F. Moustafa, J. Magn. Magn. Mater. **320** (2008) 3356-3360.
20. K.H. Ahn, X.W. Wu, K. Liu, C.L. Chien, Phys. Rev. B **54**(1996) 15299-15302. J. Appl. Phys. **81** (1997) 5505.
21. J. Gutierrez, A. Pena, J. M. Barandiaran, J. L. Pizarro, T. Hemandez, L. Lezama, M. Insausti, T. Rojo, Phys. Rev. B **61** (2000) 9028-9035.
22. W. Boujelben, A. Cheikh-Rouhou, J. Pierre, J. C. Joubert, J. Alloy. Compd. **314** (2001) 15-21.
23. F. Rivadulla, M.A. Lo´pez-Quintela, L.E. Hueso, C. Jardo´n, A. Fondado, J. Rivas, M.T. Causac, R.D. Sánchez, Solid State Commun., **110** (1999) 179–183.
24. S. Bhattacharya, S. Pal, R.K. Mukherjee, B.K. Chaudhuri, S. Neeleshwar, Y.Y. Chen, S. Mollah, H.D. Yang, J. Magn. Magn. Mater. **269** (2004) 359-371